Oxygen Sensing

DOI: 10.1002/ange.201405048

Targetable Phosphorescent Oxygen Nanosensors for the Assessment of Tumor Mitochondrial Dysfunction By Monitoring the Respiratory Activity**

Xiao-Hui Wang, Hong-Shang Peng, Lin Yang, Fang-Tian You, Feng Teng,* Ling-Ling Hou, and Otto S. Wolfbeis*

Abstract: *Cellular respiration is a worthwhile criterion to evaluate mitochondrial dysfunction by measuring the dissolved oxygen. However, most of the existing sensing strategies merely report extracellular (ec-) or intracellular (ic-) O_2 rather than intramitochondrial (im-) O_2. Herein we present a method to assess tumor mitochondrial dysfunction with three phosphorescent nanosensors, which respond to ec-, ic-, and im-O_2. Time-resolved luminescence is applied to determine the respective oxygen consumption rates (OCRs) under varying respiratory conditions. Data obtained for the OCRs and on (intra)cellular O_2 gradients demonstrate that mitochondria in tumor cells are distinctly less active than those of healthy cells, resulting from restrained glucose utilization of and physical injury to the mitochondria. We believe that such a site-resolved sensing strategy can be applied to numerous other situations, for example to evaluate the adverse effects of drug candidates.*

Mitochondria are crucial for numerous vital cellular processes, such as adenosine triphosphate (ATP) production and the initiation of apoptosis. Mitochondrial dysfunctions might not only result in disorders such as diabetes,[1] but also lead to the development of cancers.[2] Although tumor mitochondrial dysfunction has been extensively investigated in terms of cellular events, the findings are diverse and even conflicting.[3] Alternatively, mitochondrial dysfunction in cancer cells should be better evaluated from an overall viewpoint. In this context, mitochondrial respiration seems to be a very worthwhile criterion.[4]

[*] X.-H. Wang, Assoc. Prof. H.-S. Peng, L. Yang, Prof. F.-T. You, Prof. F. Teng
Key Laboratory of Luminescence and Optical Information
Ministry of Education, Institute of Optoelectronic Technology
Beijing Jiaotong University
Beijing 100044 (China)
E-mail: hshpeng@bjtu.edu.cn
fteng@bjtu.edu.cn
Assoc. Prof. L.-L. Hou
College of Life Sciences & Bioengineering
Beijing Jiaotong University, Beijing 100044 (China)
Prof. O. S. Wolfbeis
Institute of Analytical Chemistry, Chemo- and Biosensors
University of Regensburg, 93040 Regensburg (Germany)

[**] This work was financially supported by the NSFC (Grants 61078069 and 11274038), the NCET (12-0771), the NSF for Distinguished Young Scholars (61125505), and the FRFCU (2010JBZ006).

Supporting information for this article is available on the WWW under http://dx.doi.org/10.1002/anie.201405048.

The respiration rates under conditions of mitochondrial dysfunction have been determined using Clark-type oxygen electrodes[5] and fluorescence-based methods.[6] However, these detection techniques suffer from low time/space resolution, because the measured oxygen concentrations are average values for the whole extracellular (ec) or intracellular (ic) space. Such a poor spatial resolution precludes these methods from specifically monitoring respiratory activity. This problem may be circumvented by monitoring the respiratory activity of isolated mitochondria,[7] but in this case the communication with the outer cellular environment is blocked and this could result in biased information. Therefore, techniques that can exclusively detect intramitochondrial (im) O_2 in living cells are needed.

A considerable number of optical sensors for oxygen are known, mainly for purposes of detecting O_2 in biological systems.[8] Particularly, many nanosized sensors with elaborate design have been reported to sense ic-O_2[9] and even cellular O_2 gradients.[10] On the other hand, few optical probes are known that can sense im-O_2, except for two kinds of endogenous probing, i.e. using fluorescent redox indicators such as NADH[11] and the metal-free probe protoporphyrin IX (PpIX).[12] Unfortunately, the NADH probe does not enable O_2 to be determined directly and quantitatively, whilst PpIX can measure im-O_2 but its endogenous synthesis may disturb mitochondrial biosynthetic processes and as a result alter the status of mitochondrial function. The group of Tobita[12c] has designed a mitochondria-specific molecular iridium probe (rather than nanoparticles) containing two benzothienylpyridinato groups and an acetylacetone ancillary ligand bearing a triphenylphosphonium group. The phosphorescence of the probe is strongly quenched by oxygen in the mitochondria of HeLa cells.

Previously, we have prepared poly-L-lysine (PLL) coated O_2 nanosensors based on quenched phosphorescence.[13] When such nanoparticles (NPs) are covalently conjugated to the known[14] mitochondriotropic ligand triphenylphosphonium (TPP), the resulting NPs can specifically target mitochondria.[15] Hence, we propose that TPP-conjugated nanosensors may enable an accurate measurement of respiration rate, because they respond to im-O_2 only and do not interfere with other mitochondrial (bio)processes. Specifically, we describe here three kinds of phosphorescent O_2 nanosensors capable of assessing tumor mitochondrial dysfunction. The nanosensors possess the same sensing particle core, but differ in particle surface and respond to ec-O_2, ic-O_2, and im-O_2. These three targetable nanosensors are employed, along with

time-resolved luminescence using a plate reader, to study the cellular respiration of HepG2 cells (a human hepatocellular liver carcinoma cell line) and a normal human liver cell line for comparison.

The sensing NPs were prepared by modified encapsulation–reprecipitation methods as described in the Supporting Information (SI).[13,15,16] The resulting NPs possess a hydrophobic hybrid core made from polystyrene (PS) and dodecyltrimethoxysilane (DTS) and are randomly doped with the O_2 probe Pt^{II}-*meso*-tetra(pentafluorophenyl)porphine (PtTFPP). However, their surfaces are entirely different. Particles prepared in the absence of PLL are covered with a thin shell of silica (Si-NPs). The Si-NPs are negatively charged due to surface silanol groups; they cannot pass membranes and thus remain in the extracellular space. When the synthesis is performed in the presence of PLL, the resulting particles are covered with a layer of PLL (PLL-NPs). The PLL-NPs, in contrast, are positively charged due to surface amino groups, thereby ensuring an easy cellular uptake. The subsequent conjugation of TPP groups to the surface of the PLL-NPs endows them with mitochondrial targeting groups (TPP-NPs). The lipophilic TPP-NPs bear large-area-dispersed cationic charges,[14a] which largely facilitate their passage through the lipid bilayer of mitochondria (note: the transmembrane potential $\Delta\psi$ typically is up to 200 mV) and the final accumulation within the mitochondrial matrix.[14b,15,17] Cross-sections of the three sensing NPs are schematically depicted in Figure 1 a.

SEM images of Si-NPs, PLL-NPs, and TPP-NPs in Figure 1 b show that their average diameters are about 51, 77, and 67 nm, respectively. This is consistent with the hydrodynamic sizes obtained by dynamic light scattering (see Figure S1). The zeta potentials are −17.5, +51.6, and +47.1 mV (Figure 1 c), corresponding to the SiO_2, PLL, and TPP surfaces, respectively. Figure 1 d shows emission spectra of TPP-NPs at various O_2 concentrations. The 650 nm emission of the probe PtTFPP is highly sensitive to O_2, showing a quenching response of 87% in intensity when changing from O_2-free water to O_2-saturated water. Because of the identical sensing core, the Si-NPs and PLL-NPs exhibit similar oxygen-sensitive emissions (Figure S2).

Cellular localizations of the three targetable nanosensors were studied with confocal microscopy, as shown in Figure 2 a. The cells are additionally stained with MitoTracker Red (MTR) to indicate mitochondria and the contours of the cells. To avoid interference with MTR, the PtTFPP in the NPs was replaced with the green fluorescent dye coumarin 6 (C6) (Figure S3). By looking only at the green channels one can see that both the PLL- and the TPP-NPs are readily taken up by cells, whereas the Si-NPs are cell-impermeable. The overlay channels (red and green) reveal that the PLL- and TPP-NPs both localize in the mitochondrial compartments as evidenced by the clear yellow signals, corresponding to the colocalization of the red and green signals. There is a major difference, however, in that the PLL-NPs nonspecifically interact with cellular organelles due to the positively charged amino groups, whereas the TPP-NPs selectively target mitochondria.[15,17]

To further confirm that the TPP-NPs are mainly located in the mitochondria rather than in their close proximity, ultrathin sections of loaded HepG2 cells were characterized by transmission electron microscopy (TEM, Figure 2 b). The result clearly indicates that the TPP-NPs (black particles) mainly reside within the mitochondria, which are outlined in red. For comparison, the three nanosensors were also investigated with LO2 cells, and similar results were obtained (Figure S4). We conclude that the Si-, PLL-, and TPP-NPs are appropriate means to sense ec-, ic-, and im-O_2, respectively, in both cancer and healthy cells, as illustrated in Figure 2 c.

In vivo calibration plots were established for the determination of ec-, ic- and im-O_2 in both HepG2 cells and LO2 cells using the time-resolved fluorescence microplate reader. Because the sensing core is the same in all cases, a common calibration plot (type of exponential decay function) is constructed for the three nanosensors for each cell type (Figure S5) to convert the lifetime readings into O_2 concentrations.

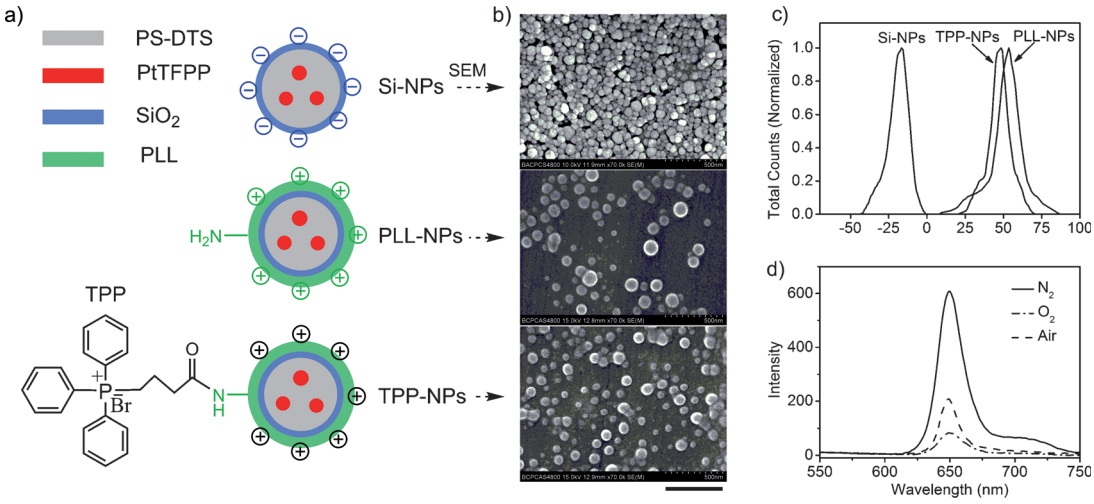

Figure 1. a) Cross-section of nanoparticles Si-, PLL-, and TPP-NPs (not to scale). The probe PtTFPP is randomly doped in the hybrid core (PS-DTS), and the particle surface is covered with either a silica layer, a PLL layer, or TPP groups. b) SEM images (scale bar: 500 nm) and c) zeta potentials. d) Emission spectra of TPP-NPs under 400 nm excitation in aqueous solutions equilibrated with nitrogen, air, and oxygen.

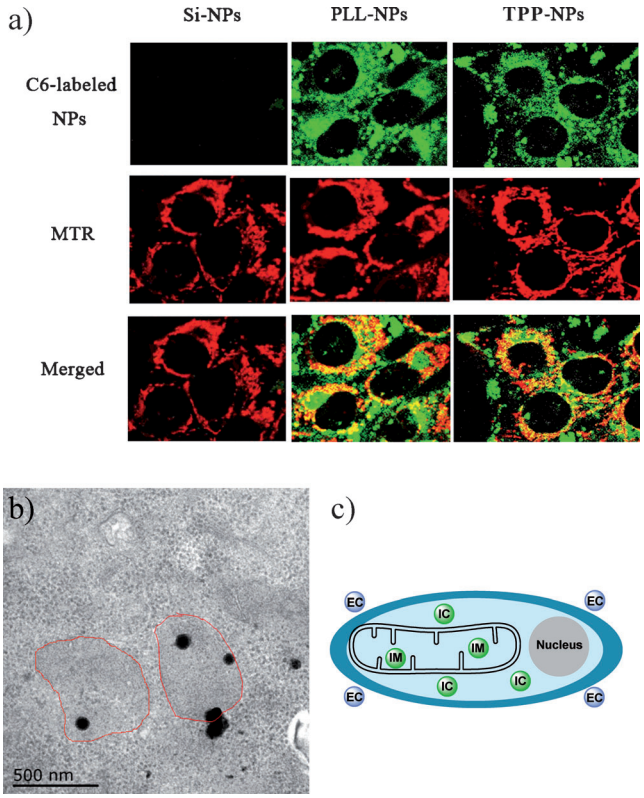

Figure 2. a) Confocal fluorescence images of HepG2 cells treated with Si-NPs (left), PLL-NPs (middle), and TPP-NPs (right). Cells are viewed in the green channel for C6-labeled NPs (excitation 405 nm, emission 480–520 nm) and the red channel for MTR (excitation 534 nm, emission 580–620 nm), respectively. b) TEM image of an ultrathin section of HepG2 cells loaded with TPP-NPs (80 nm in thickness). The red line outlines the contour of separate mitochondria. c) Schematic distribution of Si- (EC), PLL- (IC), and TPP-NPs (IM) located in the ec-, ic- and im-volume, respectively.

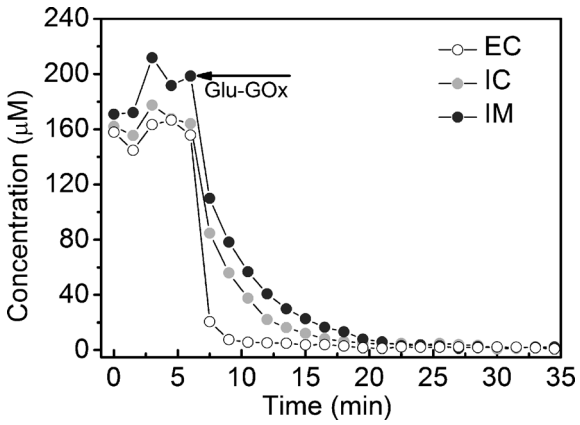

Figure 3. Response of Si-NPs (EC), PLL-NPs (IC), and TPP-NPs (IM) to cellular O_2 gradients. After equilibration with air for 20 min, cellular O_2 was depleted by addition of glucose and GOx at the time indicated by an arrow.

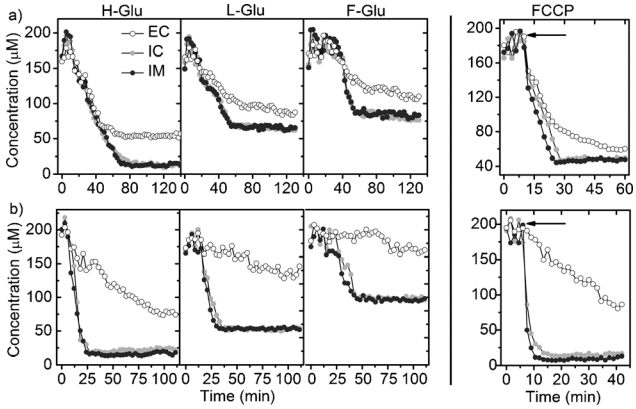

Figure 4. Time-dependent cellular O_2 concentrations (μM) of a) HepG2 and b) LO2 cells equilibrated with various glucose levels (left panel) and FCCP (right panel). The cells are monitored with ec-, ic-, and im-nanosensors for O_2, respectively. After initial cell adaption (for glucose, $t = 0$; for FCCP, time is indicated by the arrows), the culture medium was either replaced by fresh Dulbecco's modified Eagle medium (DMEM) with a high glucose concentration (H-Glu, 4500 mg L^{-1}), a low glucose concentration (L-Glu, 1000 mg L^{-1}), and glucose-free (F-Glu), respectively, or treated with FCCP (10 μL of 40 μM stock solution per well).

The in vivo response time is another crucial parameter when using such nanosensors. To guarantee a good temporal resolution, the localized nanosensors are expected to promptly respond to dissolved O_2. Otherwise, the subtle changes of mitochondrial respiration may not be correctly reported. To achieve this, dynamic O_2 gradients were artificially established by addition of glucose and glucose oxidase (GOx), a system that quickly consumes all dissolved O_2 through the oxidation of glucose. The resulting gradients were assessed with the nanosensors for ic-, ec-, and im-O_2. Figure 3 shows that first ec-O_2 is consumed, followed by ic-O_2 and finally im-O_2. This experiment nicely demonstrates that (intra)cellular O_2 gradients can be detected in real-time by the three targetable nanosensors.

In tumor cells, the mitochondrial pathway of glucose usage (through aerobic respiration) is suppressed and widely replaced by anaerobic glycolysis (often referred to as the Warburg pathway). One can therefore expect that the mitochondrial respiration (expressed by O_2 consumption) is different for cancer cells compared to normal cells in response to glucose supply. Figure 4 (left panel) displays time traces of the respiratory activities of HepG2 and LO2 cells treated with different quantities of glucose. A large decrease in the concentrations of ec-, ic- and im-O_2 is observed as a result of the consumption of glucose (until an equilibrium is reached), but the rates of deoxygenating are different as manifested by the presence of cellular O_2 gradients between ec- and ic- (or im-) pools. Obviously, the nanosensors for ic- and im-O_2 can report the respiratory activity better than the ec-O_2 nanosensors.

By defining oxygen consumption rates (OCRs) as the difference in the concentration between initial and equilibrium states versus the elapsed time, that is, $R = \Delta C[O_2]/\Delta t$, the glucose-dependent OCRs can be calculated (listed in Table S1). In a first approximation, the OCR of im-O_2 (R_{im}) in LO2 cells is three times higher than that in HepG2 cells in the case of high glucose concentration (H-Glu), but only two times higher in the case of low glucose concentration (L-Glu),

and the same under glucose-free conditions (F-Glu). When the supply of glucose is reduced from H-Glu to F-Glu, the R_{im} in LO2 cells slows down by a factor of 7.4, but is only slightly affected in HepG2 cells. These discrepancies in OCRs can be easily identified in the histogram shown in Figure 5.

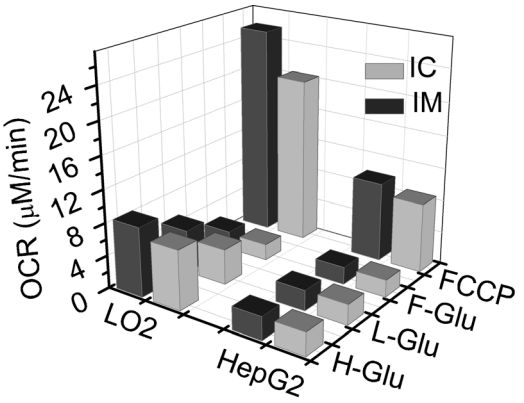

Figure 5. Consumption rates of ic-O_2 and im-O_2 in HepG2 and LO2 cells, respectively. The data were calculated from Figure 4.

Given that im-O_2 is in dynamic equilibrium with ic-O_2 and with O_2 consumed by respiration, it is plausible to assume that R_{im} is directly related to the mitochondrial respiration rate. Hence the glucose-dependent R_{im} provides additional support for the finding that the mitochondrial pathway of glucose utilization is indeed restrained in tumor cells, and that the mitochondrial respiration in tumor cells is less active than in healthy ones. Owing to the suppressed glucose utilization in tumor cells, the R_{im} is less dependent on glucose.

For the above glucose-controlled respiration, the mitochondrial inactivity is more likely to result from a down-regulated pathway of glucose usage than from mitochondrial defects. To amplify the effects of mitochondrial defects on respiratory activities, the cells were treated with the mitochondrial uncoupler carbonylcyanide-*p*-trifluoromethoxyphenylhydrazone (FCCP) which is known to stimulate the respiratory chain directly. The resulting dynamic cellular O_2 concentrations were measured with the nanosensors and are plotted in Figure 4 (right panel). It was observed that intracellular O_2 gradients are established between ic- and im-pools in both HepG2 and LO2 cells. It appears that the mitochondrial respiration in tumor cells is stimulated to a more active status so that the inward diffusion of ic-O_2 cannot keep pace with the consumption of im-O_2. On the other hand, the successful detection of the presence of large ic-O_2 gradients indicates that nanosensors targeted to mitochondria represent a very powerful means to quantify the mitochondrial respiration.

The OCRs of ic- and im-O_2 were calculated (Table S1) and are plotted in Figure 5. It can be seen that both R_{im} rates of the two cell types are considerably enhanced (about three times of the corresponding OCR at the H-Glu levels) upon stimulation with FCCP. However, the R_{im} in LO2 cells is still faster by a factor of 2.5 than that in HepG2 cells, thus proving again that the respiration of mitochondria in tumor cells is much slower than in healthy cells even with addition of FCCP. Disregarding the effects of glucose uptake, this can be reasonably interpreted in terms of physically defective or impaired tumor mitochondria that are not capable of supporting a fast respiration rate as healthy mitochondria are able to do.

In summary, three targetable O_2 nanosensors were prepared and the cellular respiration of HepG2 and LO2 cells was monitored based on the nanosensors' time-resolved luminescence. In comparison to the OCR of ec-O_2 and ic-O_2, the OCR of im-O_2 displays a sharp contrast between the mitochondrial function of tumor and healthy cells. By inspection of the data of OCRs and (intra)cellular O_2 gradients, the mitochondria in tumor cells were found to be distinctly less active than those in healthy cells. The reduced activity of tumor mitochondria is attributed not only to restrained glucose utilization but also to physical defects in the respiratory chain. We are convinced that this kind of site-resolved sensing strategy can also be applied to evaluate drug-induced mitochondrial toxicity[7c] and the efficacy of mitochondria-targeted drugs.

Please note: Minor changes have been made to this manuscript since its publication in *Angewandte Chemie* Early View. The Editor.

Received: May 10, 2014
Published online: July 7, 2014

Keywords: luminescence · mitochondrial dysfunction · nanoparticles · oxygen · sensors

[1] D. C. Wallace, *Science* **1999**, *283*, 1482.
[2] a) J. S. Modica-Napolitano, K. K. Singh, *Mitochondrion* **2004**, *4*, 755; b) G. Kroemer, J. Pouyssegur, *Cancer Cell* **2008**, *13*, 472; c) L. Galluzzi, E. Morselli, O. Kepp, I. Vitale, A. Rigoni, E. Vacchelli, M. Michaud, H. Zischka, M. Castedo, G. Kroemer, *Mol. Aspects Med.* **2010**, *31*, 1.
[3] a) D. C. Wallace, *Nature* **2012**, *12*, 685; b) P. Koivunen, S. Lee, C. G. Duncan, G. Lopez, G. Lu, S. Ramkissoon, J. A. Losman, P. Joensuu, U. Bergmann, S. Gross, J. Travins, S. Weiss, R. Looper, K. L. Ligon, R. G. W. Verhaak, H. Yan, W. G. Kaelin, Jr., *Nature* **2012**, *483*, 484.
[4] M. D. Brand, D. G. Nicholls, *Biochem. J.* **2011**, *435*, 297.
[5] a) B. Chance, G. R. Williams, *J. Biol. Chem.* **1955**, *217*, 383; b) C.-C. Wu, H.-N. Luk, Y.-T. T. Lin, C.-Y. Yuan, *Talanta* **2010**, *81*, 228.
[6] a) R. R. Deshpande, E. Heinzle, *Biotechnol. Lett.* **2004**, *26*, 763; b) A. A. Gerencser, A. Neilson, S. W. Choi, U. Edman, N. Yadava, R. J. Oh, D. A. Ferrick, D. G. Nicholls, M. D. Brand, *Anal. Chem.* **2009**, *81*, 6868.
[7] a) Y. Will, J. Hynes, V. I. Ogurtsov, D. B. Papkovsky, *Nat. Protoc.* **2007**, *1*, 2563; b) A. Heller, L. H. Fischer, O. S. Wolfbeis, A. Goepferich, *Exptl. Cell Res.* **2012**, *318*, 1667; c) J. Hynes, L. D. Marroquin, V. I. Ogurtsov, K. N. Christiansen, G. J. Stevens, D. B. Papkovsky, Y. Will, *Toxicol. Sci.* **2006**, *92*, 186.
[8] X. D. Wang, O. S. Wolfbeis, *Chem. Soc. Rev.* **2014**, *43*, 3666.
[9] a) Y. E. L. Koo, Y. F. Cao, R. Kopelman, S. M. Koo, M. Brasuel, M. A. Philbert, *Anal. Chem.* **2004**, *76*, 2498; b) C. Wu, B. Bull, K. Christensen, J. McNeill, *Angew. Chem.* **2009**, *121*, 2779; *Angew. Chem. Int. Ed.* **2009**, *48*, 2741; c) Y.-E. K. Lee, E. E. Ulbrich, G. Kim, H. Hah, C. Strollo, W. Fan, R. Gurjar, S. M. Koo, R. Kopelman, *Anal Chem.* **2010**, *82*, 8446; d) X. D. Wang, J. A. Stolwijk, T. Lang, M. Sperber, R. J. Meier, J. Wegener, O. S. Wolfbeis, *J. Am. Chem. Soc.* **2012**, *134*, 17011.

[10] a) A. V. Kondrashina, R. I. Dmitriev, S. M. Borisov, I. Klimant, I. O'Brien, Y. M. Nolan, A. V. Zhdanov, D. B. Papkovsky, *Adv. Funct. Mater.* **2012**, *22*, 4931; b) R. I. Dmitriev, A. V. Zhdanov, G. Jasionek, D. B. Papkovsky, *Anal. Chem.* **2012**, *84*, 2930.
[11] a) K. A. Foster, C. J. Beaver, D. A. Turner, *Neuroscience* **2005**, *132*, 645; b) K. A. Foster, F. Galeffi, F. J. Gerich, D. A. Turner, M. Müller, *Prog. Neurobiol.* **2006**, *79*, 136.
[12] a) E. G. Mik, J. Stap, M. Sinaasappel, J. F. Beek, J. A. Aten, T. G. van Leeuwen, C. Ince, *Nat. Methods* **2006**, *3*, 939; b) S. I. A. Bodmer, G. M. Balestra, F. A. Harms, T. Johannes, N. J. H. Raat, R. J. Stolker, E. G. Mik, *J. Biophotonics.* **2012**, *5*, 140 – 151; c) T. Murase, T. Yoshihara, S. Tobita, *Chem. Lett.* **2012**, *41*, 262 – 263.
[13] X. H. Wang, H. S. Peng, H. Ding, F.-T. You, S.-H. Huang, F. Teng, B. Dong, H.-W. Song, *J. Mater. Chem.* **2012**, *22*, 16066.
[14] a) M. P. Murphy, *Biochim. Biophys. Acta Bioenerg.* **2008**, *1777*, 1028; b) S. Biswas, N. S. Dodwadkar, A. Piroyan, V. P. Torchilin, *Biomaterials* **2012**, *33*, 4773.
[15] X. H. Wang, H. S. Peng, L. Yang, et al., *J. Mater. Chem. B* **2013**, *1*, 5143 – 5152.
[16] H. S. Peng, M. I. J. Stich, J. B. Yu, L.-N. Sun, L. H. Fischer, O. S. Wolfbeis, *Adv. Mater.* **2010**, *22*, 716.
[17] S. Marrachea, S. Dhar, *Proc. Natl. Acad. Sci. USA* **2012**, *109*, 16288.

